Structures and Thermochemistry of the Alkali Metal Monoxide Anions, Monoxide Radicals, and Hydroxides

Benjamin Mintz,[†] Bun Chan,[§] Michael B. Sullivan,[‡,⊥] Thomas Buesgen,[‡,¶] Anthony P. Scott,[‡] Steven R. Kass,[#] Leo Radom,*[,‡,§] and Angela K. Wilson*[,†]

Center for Advanced Scientific Computing and Modeling (CASCaM), Department of Chemistry, University of North Texas, Denton, Texas 76203-5070, School of Chemistry and Centre of Excellence for Free Radical Chemistry and Biotechnology, University of Sydney, Sydney, NSW 2006, Australia, Research School of Chemistry, Australian National University, Canberra, ACT 0200, Australia, and Department of Chemistry, University of Minnesota, Minneapolis, Minnesota 55455-0431

Received: April 16, 2009; Revised Manuscript Received: July 9, 2009

The geometries, enthalpies of formation (ΔH^o_f), separations of electronic states, electron affinities, gas-phase acidities, and bond dissociation energies associated with the alkali metal monoxide anions (MO^-), monoxide radicals ($MO^•$), and hydroxides (MOH) (M = Li, Na, and K) have been investigated using single-reference and multireference variants of the W*n*C procedures. Our best estimates of the ΔH^o_f values for the ground states at 298 K are as follows: 8.5 ($^3\Pi$ LiO^-), 48.5 ($^2\Pi$ $LiO^•$), −243.4 ($^1\Sigma^+$ LiOH), 34.2 ($^3\Pi$ NaO^-), 86.4 ($^2\Pi$ $NaO^•$), −190.8 ($^1\Sigma^+$ NaOH), 15.1 ($^1\Sigma^+$ KO^-), 55.9 ($^2\Sigma^+$ $KO^•$), and −227.0 ($^1\Sigma^+$ KOH) kJ mol^{-1}. While the $LiO^•$ and $NaO^•$ radicals have $^2\Pi$ ground states, for $KO^•$, the $^2\Sigma^+$ and $^2\Pi$ electronic states lie very close in energy, with our best estimate being a preference for the $^2\Sigma^+$ state by 1.1 kJ mol^{-1} at 0 K. In a similar manner, the ground state for MO^- changes from $^3\Pi$ for LiO^- and NaO^- to $^1\Sigma^+$ for KO^-. The $^1\Sigma^+$ state of KO^- is indicated by the calculated $\mathscr{T}_1$ diagnostic and the SCF contribution to the total atomization energy to have a significant degree of multireference character. This leads to a difference of more than 100 kJ mol^{-1} between the single-reference W2C and multireference W2C-CAS-ACPF and W2C-CAS-AQCC estimates for the $^1\Sigma^+$ ΔH^o_f for KO^-.

1. Introduction

Alkali metal monoxides and hydroxides play an important role in a wide range of areas.[1−7] For example, $NaO^•$ ($A^2\Sigma^+$) is the chain carrier for Na (^2P) production in the mesosphere.[8] Also, in high-temperature combustion, the presence of alkali metal monoxides and hydroxides is a known cause of corrosion in high-temperature industrial reactor components.[9−11] These and many other important applications have led to an interest in the characterization of the alkali metal monoxides and hydroxides. Unfortunately, there is little or no gas-phase experimental information currently available for the enthalpies of formation (ΔH^o_f) for many of these species, and some of the reported values, such as for the ΔH^o_f for the $KO^•$ radical (71.13 ± 42 kJ mol^{-1}),[12] have large uncertainties. This limited amount of experimental data has encouraged many computational studies on the alkali metal monoxides and hydroxides.[13−33]

One of the most thoroughly studied and still unresolved problems for the alkali metal monoxides relates to the ground state of the $MO^•$ radicals. Although experimental[25,34−40] and theoretical[15−17,19,23,24,28,29] studies have shown that the ground state changes from $^2\Pi$ to $^2\Sigma^+$ as the size of the alkali metal increases, agreement has not yet been reached as to where this crossover occurs. Thus, while both experimental and theoretical studies agree that the ground states of $NaO^•$ and $RbO^•$ are $^2\Pi$ and $^2\Sigma^+$, respectively,[15−17,25,36,37,39,40] there is no clear consensus yet about the ground state of $KO^•$. For instance, while an early magnetic deflection experiment pointed to a $^2\Sigma^+$ ground state for $KO^•$,[34,36] a microwave spectroscopic study has suggested that the ground state of $KO^•$ is $^2\Pi$.[41]

One of the earliest theoretical studies on the alkali metal monoxides employing the Hartree−Fock method indicated a $^2\Pi$ ground state for $NaO^•$ and a $^2\Sigma^+$ ground state for $KO^•$ and $RbO^•$,[15] in agreement with the magnetic deflection experiment.[34,36] In contrast, Allison et al. later reported that the ground state of $KO^•$ is $^2\Pi$ at the CISD level.[16] However, it has been suggested that the valence-double-ζ basis set used in their study was too small, which could lead to large basis set superposition errors (BSSE) and an incorrect prediction of the ground state for $KO^•$.[21]

More recently, Lee et al. carried out a comprehensive study of the $KO^•$ radical using the CCSD(T) method in combination with basis sets up to sextuple-ζ in size.[31] They found that when spin−orbit coupling is not considered, the $^2\Pi$ and $^1\Sigma^+$ potential energy curves cross near their minimum energies. However, when spin−orbit coupling is considered, an avoided crossing occurs between the $^2\Pi$ and $^2\Sigma^+$ (actually $^2\Pi_{1/2}$ and $^2\Sigma^+_{1/2}$) potential energy curves. This leads to the lowest-energy state of the $KO^•$ radical being the $^2\Sigma^+_{1/2}$ state at short bond distances but the $^2\Pi_{1/2}$ state at large bond distances.

Prior to the study of Lee et al., Bauschlicher et al. examined the ground and low-lying states of $MO^•$ radicals and MO^- anions (where M = Li, Na, and K)[24] using multireference configuration interaction calculations that included single and double excitations, as well as a size-consistency correction (MRCI+Q).[42]

* To whom correspondence should be addressed. E-mail: radom@chem.usyd.edu.au (L.R.); akwilson@unt.edu (A.K.W.).
† University of North Texas.
§ University of Sydney.
‡ Australian National University.
# University of Minnesota.
¶ Current address: Bayer Material Science AG, Leverkusen, Germany.
⊥ Current Address: Institute of High Performance Computing, Singapore.

10.1021/jp9034826 CCC: $40.75
Published on Web 08/03/2009

TABLE 1: Orbitals Included in the Correlation Space Defined as Relaxed Valence for Nonmetals (rv) and Relaxed Inner Valence for Alkali Metals (riv)[a]

	frozen	active
	rv	
O	1s	2s, 2p
H		1s
	riv	
Li		1s, 2s, 2p
Na	1s	2s, 2p, 3s, 3p
K	1s, 2s, 2p	3s, 3p, 4s, 4p

[a] This correlation space was used in ref 67.

They concluded that the ground state of KO• is $^2\Sigma^+$, with the $^2\Pi$ state lying 2.2 kJ mol^{-1} higher in energy. Their study also found that the ground state for the anions changes from $^3\Pi$ to $^1\Sigma^+$ as the size of the alkali metal increases. While the ground states of LiO^- and KO^- were found to be $^3\Pi$ and $^1\Sigma^+$, respectively, the study was inconclusive about the ground state of NaO^-.

These previous studies have shown that the theoretical prediction of energy-related properties for the alkali metal monoxide radicals and anions is not entirely straightforward and in some cases may require the use of multireference methods combined with large basis sets.[20] Unfortunately, this can become computationally very demanding in terms of memory, disk space, and CPU time requirements. Therefore, we have investigated the use of high-level composite approaches in the present study.

The philosophy of the composite methods is to combine a series of results from computationally simpler ab initio methods in order to approximate results for a more accurate but computationally more expensive approach. Notable examples of composite methods include the Gaussian theories (G*n*),[43−48] the complete basis set methods (e.g., CBS-QB3),[49−51] the Weizmann methods (W*n*),[52−55] the HEAT method,[56,57] and the correlation-consistent composite approach (ccCA).[58−62] The present study investigates the use of several modified versions of the W*n* methods, which were chosen because of their ability to achieve accuracies of ∼1 kJ mol^{-1} for many thermochemical properties.[52,53] Additionally, the W*n* methods have been adapted to incorporate multireference procedures,[63−65] which may be necessary for some of the systems that will be studied.[31]

In previous studies of the alkali metal and alkaline earth metal compounds, it was found that standard implementations of composite methods are sometimes not sufficient. For example, Schulz et al.[66] found examples where the standard G2 method performed poorly, with errors greater than 100 kJ mol^{-1}. They found that by extending the correlation space, using CCSD(T) instead of QCISD(T), and performing CCSD(T)/6-311+G-(3df,2p) calculations without additivity approximations, the large errors obtained in the G2 calculations can be minimized. In another study, Sullivan et al. found that the use of a similar combination of a relaxed-inner-valence (riv) correlation space for the metal and a relaxed-valence (rv) correlation space for the oxygen (Table 1) was also important for the G3 method.[67] However, Sullivan et al. found that the (riv,rv) correlation space led to spectacular failures for the W*n* methods, with discrepancies from accurate experimental values in excess of 90 kJ mol^{-1} in some cases. The failures in the W*n* methods when combined with the (riv,rv) correlation space were found to be associated with the use of the standard Dunning correlation-consistent basis sets (cc-pV*n*Z),[68−71] which were not designed to describe the inner-valence region that was being relaxed. To compensate for this need, Sullivan et al. used core−valence basis sets, cc-pWCV*n*Z (denoted as WCV*n*Z to distinguish them from the existing cc-pCV*n*Z[72,73] and cc-pwCV*n*Z[74] basis sets), developed by Martin,[75] in modified methods denoted as W*n*C. The W*n*C methods, which use the (riv,rv) correlation space, showed significant improvements in performance over the W*n* (riv,rv) methods. For example, W1C predicts a ΔH^o_f value of −189.6 kJ mol^{-1} for NaOH,[67] which is significantly closer to the value of −197.76 kJ mol^{-1} in the JANAF tables[12] than the W1 (riv,rv) value of −286.9 kJ mol^{-1}.

In the present study, we examine the performance of the W*n*C methods in describing alkali metal monoxide anions (MO^-), monoxide radicals (MO•), and hydroxides (MOH). The structures and selected thermochemical properties of MO^-, MO•, and MOH (M = Li, Na, and K) have been investigated. Specifically, we examine (a) the structures for all of these species, (b) the enthalpies of formation for all of these species, (c) the state separations for MO^- and MO•, (d) the electron affinities for MO•, and (e) the bond dissociation energies and gas-phase acidities for MOH.

2. Theoretical Procedures

All calculations were carried out with the GAUSSIAN 03[76] or MOLPRO 2002.6[77] program packages. Enthalpies of formation were obtained using the atomization method.[78]

Geometries were determined by calculating the potential energy curves for each of the states of MO^- and MO• (where M = Li, Na, and K). A standard Dunham analysis[79] was then performed to determine the optimal bond distances for the MO^- and MO• species. For the alkali metal hydroxides, standard geometry optimizations were performed. Frequency calculations were carried out using B3LYP/A′WCV5Z to obtain zero-point vibrational energies (ZPVE) and enthalpy temperature corrections ($\Delta\Delta H_f$) for the determination of the enthalpies of formation at 298 K ($\Delta H^\circ_{f,298}$), where A′WCV*n*Z represents the aug′-cc-pWCV*n*Z basis set. The aug′ prefix indicates that diffuse functions are not included on hydrogen or the alkali metal atoms. The vibrational frequencies were scaled by 0.985 in accordance with the standard W1 and W2 prescriptions.[52,53]

The current study employed slightly altered versions of the W*n*C methods.[75] For the W1C method, B3LYP/A′WCV5Z geometries were used. CCSD single-point calculations were then performed with the A′WCVQZ basis set, while CCSD(T) calculations were performed with the A′WCVDZ and A′WCVTZ basis sets. The SCF, CCSD, and triple excitation (T) components of the CCSD(T) total energy are all separately extrapolated to obtain CBS limits for each component, as discussed in previous studies.[52,53]

For the W2C method, CCSD(T)/A′WCV5Z and CCSD(T)/AA′WCV5Z geometries were used, where AA′WCV*n*Z denotes the aug-aug′-cc-pWCV*n*Z basis set, which includes diffuse functions on all atoms except hydrogen, that is, diffuse functions were now included on the alkali metal atoms M. The procedure for obtaining the CCSD(T) CBS limit is similar to that for W1C, except that larger basis sets (*n* = T, Q, 5 as opposed to D, T, Q) are employed for the single-point calculations. The (riv,rv) correlation space (Table 1) was used for all W*n*C methods.

Core correlation was obtained by taking the difference in CCSD(T)/MTsmall energies with and without the core electrons frozen, and this was added to the CCSD(T) CBS limit. Scalar relativistic corrections were added, obtained as the averaged coupled-pair functional (ACPF)[80,81] expectation values of the first-order Darwin and mass−velocity operators.[82,83] The 1s

TABLE 2: Optimized Geometries for MO^-, $MO^\bullet$, and MOH (Å)

molecule	state	B3LYP/ A′WCV5Z	B3LYP/ AA′WCV5Z	CCSD(T)/ A′WCV5Z	CCSD(T)/ AA′WCV5Z	MRCI+Q/ A′WCV5Z	MRCI+Q/ AA′WCV5Z	exptl
LiO^-	$^1\Pi$	1.752	1.742	1.755	1.746	1.759	1.749	
	$^1\Sigma^+$	1.606	1.606	1.647	1.648	1.697	1.687	
	$^3\Pi$	1.752	1.742	1.755	1.746	1.752	1.747	
	$^3\Sigma^+$	1.667	1.655	1.671	1.659	1.670	1.660	
$LiO^\bullet$	$^2\Pi$	1.684	1.684	1.689	1.689	1.689	1.689	1.688[a]
	$^2\Sigma^+$	1.588	1.588	1.591	1.591	1.591	1.591	1.599[b]
LiOH	r(Li−O)	1.577	1.577	1.580	1.580	1.580	1.580	1.5816(10)[c]
	r(O−H)	0.950	0.950	0.949	0.949	0.949	0.948	0.9691(21)[c]
NaO^-	$^1\Pi$	2.152	2.141	2.138	2.134	2.142	2.137	
	$^1\Sigma^+$	2.003	2.003	1.979	1.977	2.045	2.044	
	$^3\Pi$	2.153	2.144	2.140	2.134	2.144	2.138	
	$^3\Sigma^+$	2.063	2.056	2.050	2.044	2.048	2.043	
$NaO^\bullet$	$^2\Pi$	2.060	2.060	2.054	2.054	2.053	2.054	2.052[d]
	$^2\Sigma^+$	1.956	1.956	1.952	1.952	1.952	1.952	1.95[b]
NaOH	r(Na−O)	1.943	1.943	1.940	1.939	1.940	1.939	1.95(2)[c]
	r(O−H)	0.952	0.952	0.951	0.952	0.951	0.952	
KO^-	$^1\Pi$	2.441	2.424	2.437	2.420	2.443	2.422	
	$^1\Sigma^+$	2.194	2.187	2.037	1.998	2.283	2.268	
	$^3\Pi$	2.444	2.426	2.438	2.421	2.440	2.417	
	$^3\Sigma^+$	2.288	2.270	2.281	2.263	2.284	2.265	
$KO^\bullet$	$^2\Pi$	2.322	2.322	2.324	2.324	2.326	2.327	2.321[d]
	$^2\Sigma^+$	2.168	2.168	2.171	2.171	2.174	2.174	2.168[d]
KOH	r(M−O)	2.202	2.202	2.202	2.202	2.201	2.202	2.196(3)[c]
	r(O−H)	0.956	0.956	0.955	0.955	0.954	0.955	0.960(10)[c]

[a] Reference 88. [b] Reference 90. [c] Reference 89. [d] Reference 39.

orbital on second- and third-row atoms was held frozen for all core correlation and scalar relativistic calculations.

For simplicity, these methods are referred to hereafter as W1C//BA, W2C//CA, and W2C//CAA, where //BA, //CA, and //CAA represent geometries optimized at the B3LYP/A′WCV5Z, CCSD(T)/A′WCV5Z, and CCSD(T)/AA′WCV5Z levels, respectively.

Our calculated values for the $\mathcal{T}_1$ diagnostic[84] and the percent SCF contribution to the total atomization energy[64] suggest that some species in the present study might possess significant multireference character. We have therefore performed additional calculations using multireference versions of the W2C procedure[63−65] to examine this possibility. Geometries are calculated at the MRCI+Q level, combined with the A′WCV5Z and AA′WCV5Z basis sets. The single-reference CCSD(T) calculations of W2C are replaced in the multireference variants by averaged coupled-pair functional (ACPF)[80,81] or averaged quadratic coupled cluster (AQCC)[85−87] calculations. The resultant methods are denoted as W2C-CAS-ACPF and W2C-CAS-AQCC, respectively (referred to as W-ACPF and W-AQCC hereafter, respectively, for simplicity).[67] The CAS parts of the calculations are carried out within a full-valence space, while the ACPF and AQCC calculations use a riv,rv correlation space.

This gives rise to four varieties of multireference W2C methods, namely, W-ACPF//MA, W-ACPF//MAA, W-AQCC//MA, and W-AQCC//MAA, where //MA and //MAA indicate the use of geometries optimized at the MRCI+Q level using the A′WCV5Z and AA′WCV5Z basis sets, respectively.

Calculated total energies at the seven theoretical levels employed in this study are presented in Table S1 of the Supporting Information.

3. Results and Discussion

3.1. Extent of Multireference Character. The $\mathcal{T}_1$ diagnostic and the percent SCF contribution to the total atomization energy are presented in Table S2 of the Supporting Information, while highlights of the results are discussed here. A value greater than 0.02 for the $\mathcal{T}_1$ diagnostic[84] or a percent SCF contribution to the total atomization energy that is smaller than 30%[55] has previously been suggested as an indicator of possible poor performance by single-reference methods due to high multireference character. We find that there are several states for which the $\mathcal{T}_1$ diagnostic is slightly larger than 0.02. Some examples include the $^3\Pi$ and $^3\Sigma^+$ states for LiO^- and KO^- for which the $\mathcal{T}_1$ diagnostic is 0.021, 0.022, 0.023, and 0.023. However, the percent SCF contribution to the total atomization energy for these states is well above the 30% threshold required for adequate single-reference character, with 39.8% for the $^3\Sigma^+$ KO^- state being the lowest. These results suggest that multireference considerations are unlikely to be an issue in these cases.

The most significant multireference diagnostics are found for the $^1\Sigma^+$ state for LiO^-, NaO^-, and KO^-, for which the percent SCF contributions to the total atomization energy are found to be −11.5, −60.4, and −54.9%, respectively, and the $\mathcal{T}_1$ diagnostic has values of 0.067, 0.045, and 0.150, respectively, utilizing CCSD(T)/AA′WCV5Z. It should be noted that while the $\mathcal{T}_1$ diagnostic and the percent SCF contributions to the total atomization energy can provide indications that multireference methods may be needed, it is not always the case that single-reference methods will fail in such cases. In fact, we will see that only the $^1\Sigma^+$ state of the KO^- anion seems to be poorly described by the single-reference procedures.

3.2. Geometries. Optimized structures for the metal oxides and hydroxides are presented in Table 2. As previously mentioned, there is only a small amount of experimental structural information[39,88−90] available for these systems, but the available data are included for comparison. Intuitively, we can expect geometries obtained at the B3LYP, CCSD(T), and MRCI+Q levels to be generally similar but to show larger discrepancies for systems with large multireference character. In such cases, the MRCI+Q method can be expected to give more reliable geometries than B3LYP and CCSD(T). Indeed, bond lengths calculated at the B3LYP, CCSD(T), and MRCI+Q

TABLE 3: Enthalpies of Formation (298 K, kJ mol^{-1}) for MO$^-$, MO$^\bullet$, and MOH (Å)

molecule	state	W1C//BA[a]	W2C//CA[b]	W2C//CAA[c]	W-ACPF//MA[d]	W-ACPF//MAA[e]	W-AQCC//MA[f]	W-AQCC//MAA[g]	best estimate	experiment
LiO^-	$^1\Pi$	18.7	18.2	16.2	13.1	9.1	12.8	8.9	11.4	
	$^1\Sigma^+$	19.2	20.8	20.6	21.0	20.1	24.5	23.7	21.9	
	$^3\Pi$	15.0	15.1	11.5	10.9	7.2	10.6	6.8	8.5	
	$^3\Sigma^+$	48.0	48.2	44.4	44.3	40.6	43.6	39.8	41.6	
$LiO^\bullet$	$^2\Pi$	51.8	52.4	52.5	47.7	47.7	45.3	45.4	48.5	84.1 ± 20.9[h] 75.3 ± 8.4[i] 69.0 ± 6.3[j]
	$^2\Sigma^+$	81.7	82.3	84.6	77.8	77.8	75.5	75.5	79.3	
LiOH	$^1\Sigma^+$	−241.8	−240.3	−240.2	−244.0	−244.0	−246.1	−246.1	−243.4	-234.3 ± 6.3[h] -238.1 ± 6[k] -228.9 ± 5.0[k] -247.0 ± 3[l] (-239 ± 5)[m]
NaO^-	$^1\Pi$	38.4	40.3	38.8	36.7	35.0	37.6	35.9	36.6	
	$^1\Sigma^+$	40.3	42.7	42.1	43.0	42.6	44.0	43.5	43.0	
	$^3\Pi$	36.4	37.5	35.9	34.5	33.0	35.2	33.7	34.2	
	$^3\Sigma^+$	58.2	59.4	58.0	56.6	55.3	57.0	55.6	56.3	
$NaO^\bullet$	$^2\Pi$	89.3	89.3	89.3	85.7	85.7	84.2	84.2	86.4	83.68[h] 87 ± 4[n]
	$^2\Sigma^+$	113.5	113.7	113.8	109.8	109.8	108.1	108.1	110.6	
NaOH	$^1\Sigma^+$	−189.6	−188.1	−188.0	−191.4	−191.3	−193.0	−192.9	−190.8	-197.76 ± 12.6[h] -191 ± 8[k] -186 ± 10[o] -193 ± 10[o] (-189 ± 5)[m]
KO^-	$^1\Pi$	28.1	28.6	23.1	24.1	18.6	24.7	18.9	20.2	
	$^1\Sigma^+$	−59.8	−107.6	−95.3	19.8	15.3	19.7	15.0	15.1	
	$^3\Pi$	26.1	27.0	21.0	23.0	17.6	23.0	17.4	18.7	
	$^3\Sigma^+$	27.9	29.2	23.0	25.6	19.5	25.5	19.1	20.5	
$KO^\bullet$	$^2\Pi$	61.6	61.1	61.2	56.2	56.3	53.6	53.7	57.0	71.13 ± 41.9[h] 65.27 ± 12.55[p] 61 ± 21[i] 59.86 ± 4.2[j]
	$^2\Sigma^+$	59.7	59.4	59.5	55.4	55.5	52.6	52.7	55.9	
KOH	$^1\Sigma^+$	−226.8	−223.5	−223.4	−227.6	−227.5	−230.1	−230.0	−227.0	-232.63 ± 3[h] -231.0[o] (-223 ± 5)[m] -229.0 ± 4[l] -228 ± 5[h]

[a] W1C//B3LYP/A′WCV5Z. [b] W2C//CCSD(T)/A′WCV5Z. [c] W2C//CCSD(T)/AA′WCV5Z. [d] W2C-CAS-ACPF//MRCI+Q/A′WCV5Z. [e] W2C-CAS-ACPF//MRCI+Q/AA′WCV5Z. [f] W2C-CAS-AQCC//MRCI+Q/A′WCV5Z. [g] W2C-CAS-AQCC//MRCI+Q/AA′WCV5Z. [h] From ref 12. [i] From ref 92. [j] From ref 93. [k] From ref 96. [l] From ref 94. [m] Recommended theoretical values from ref 67 in parentheses. [n] From ref 95. [o] From ref 9. [p] From ref 91.

levels using the AA′WCV5Z basis set are generally quite similar, with bond lengths generally lying within ~0.01 Å of one another. However, the bond lengths calculated with B3LYP and CCSD(T) for the $^1\Sigma^+$ state of MO$^-$ show quite large deviations from results obtained with MRCI+Q, which is probably a consequence of significant multireference character for the $^1\Sigma^+$ state. Thus, the B3LYP metal−oxygen bond distances differ from MRCI+Q values by 0.081, 0.041, and 0.081 Å for LiO^-, NaO^-, and KO^-, respectively, while corresponding CCSD(T) differences are 0.039, 0.067, and 0.270 Å. Overall, the mean absolute deviations (MAD) for the B3LYP/AA′WCV5Z and CCSD(T)/AA′WCV5Z geometries from MRCI+Q values are 0.012 and 0.017 Å, respectively. It should be noted that the MADs are significantly reduced when the $^1\Sigma^+$ state is omitted from the analysis, with MAD values of just 0.004 and 0.001 Å.

In comparing the performance of the B3LYP, CCSD(T), and MRCI+Q methods with the A′WCV5Z and AA′WCV5Z basis sets, we generally find differences in bond lengths that are less than 0.001 Å. However, this is not the case for the MO$^-$ anions. For example, for the KO^- anion, the AA′WCV5Z basis set gives bond lengths that are shorter than A′WCV5Z values by 0.017, 0.007, 0.018, and 0.018, respectively, for the $^1\Pi$, $^1\Sigma^+$, $^3\Pi$, and $^3\Sigma^+$ states for B3LYP, 0.017, 0.039, 0.017, and 0.018 Å, respectively, for CCSD(T), and 0.021, 0.015, 0.023, and 0.019 Å, respectively, for MRCI+Q.

3.3. Enthalpies of Formation. Our calculated enthalpies of formation (ΔH^o_f) for the alkali metal monoxide anions, monoxide radicals, and hydroxides are compared with experimental values[9,12,91−96] in Table 3. In some cases, the experimental values show significant variation among the various reported studies, and some of these values have significant uncertainties. Among our calculated values, we might expect fair agreement between our highest levels of single- and multireference methods when the systems of interest are largely single-reference. However, species with significant multireference character may give rise to larger discrepancies between the single- and multireference values. In such cases, the use of multireference approaches are likely to be more reliable.

For the present theoretical predictions, we have generally obtained our best estimated values by averaging results at the three highest levels of theory, namely, W2C//CAA, W-ACPF//MAA, and W-AQCC//MAA, which use geometries optimized at the CCSD(T) (CAA) or MRCI+Q (MAA) level with the

TABLE 4: Separations of States (0 K, kJ mol^{-1}) for MO^- and $MO^\bullet$

molecule	state	W2C//CAA[a]	W-ACPF//MAA[b]	W-AQCC//MAA[c]	best estimate	exptl
LiO^-	$^1\Pi \rightarrow {}^1\Sigma^+$	4.57	11.11	15.05	13.08	
	$^3\Pi \rightarrow {}^3\Sigma^+$	33.00	33.41	32.98	33.13	
$LiO^\bullet$	$^2\Pi \rightarrow {}^2\Sigma^+$	32.13	30.15	30.19	30.82	30.68[d]
NaO^-	$^1\Pi \rightarrow {}^1\Sigma^+$	3.54	7.36	7.47	7.42	
	$^3\Pi \rightarrow {}^3\Sigma^+$	22.07	22.37	21.94	22.13	
$NaO^\bullet$	$^2\Pi \rightarrow {}^2\Sigma^+$	24.51	24.22	23.93	24.22	24.52[d]
KO^-	$^1\Pi \rightarrow {}^1\Sigma^+$	−111.62	−3.04	−3.61	−3.33	
	$^3\Pi \rightarrow {}^3\Sigma^+$	2.04	1.93	1.80	1.92	
$KO^\bullet$	$^2\Pi \rightarrow {}^2\Sigma^+$	−1.61	−0.70	−0.92	−1.08	2.39[e]

[a] W2C//CCSD(T)/AA′WCV5Z. [b] W2C-CAS-ACPF//MRCI+Q/AA′WCV5Z. [c] W2C-CAS-AQCC//MRCI+Q/AA′WCV5Z. [d] References 39 and 88. [e] Reference 41.

AA′WCV5Z basis set. The one exception is for the $^1\Sigma^+$ state of the MO^- anions, for which the best estimates have been taken as the average of the W-ACPF//MAA and W-AQCC//MAA results. The single-reference W2C//CAA value was omitted in this case due to the potential large multireference character in these species as reflected, for example, in a difference of more than 100 kJ mol^{-1} between the single-reference and multireference ΔH^o_f values for the extreme case of the KO^- $^1\Sigma^+$ state.

Enthalpies of formation for the alkali metal hydroxides have been previously determined using high-level theoretical calculations by Sullivan et al.,[67] who recommended values of −239 ± 5, −189 ± 5, and −223 ± 5 kJ mol^{-1} for LiOH, NaOH, and KOH, respectively. These were calculated as a weighted average of their two best theoretical predictions [W2C//ACQ and G3[CC](dir,full)].[67] The best ΔH^o_f values of −243.4, −190.8, and −227.0 kJ mol^{-1}, determined in the present study for LiOH, NaOH, and KOH, respectively, agree with the values reported by Sullivan et al. to within the reported uncertainties.[67] Our values are also close to the experimental ΔH^o_f values that have the lowest reported uncertainties, showing good agreement for LiOH (−247.0 ± 3.0),[94] NaOH (−191 ± 8),[96] and KOH (−232.0 ± 3.0, −229.0 ± 4.0)[12,94] kJ mol^{-1}.

For the $MO^\bullet$ radicals, comparison of our best ΔH^o_f values with the experimental values shows that for the $^2\Pi$ state of $NaO^\bullet$, our value of 86.4 kJ mol^{-1} lies between the two experimental values (83.68 and 87 ± 4 kJ mol^{-1}).[12,95] For $KO^\bullet$, our computed ΔH^o_f of 57.0 kJ mol^{-1} lies within experimental uncertainty of the value of 59.86 ± 4.2 kJ mol^{-1}.[92] We note that JANAF lists a value for the ΔH^o_f for $KO^\bullet$ of 71.13 ± 41.9 kJ mol^{-1},[12] which is more than 10 kJ mol^{-1} above our value, and carries a large uncertainty. It seems questionable whether this is the best choice among the experimental values, given the large associated uncertainty.

The deviation between our best estimated ΔH^o_f and the experimental values is largest for the $^2\Pi$ state of the $LiO^\bullet$ radical, with the experimental values lying 20−30 kJ mol^{-1} higher than our recommended value. This large deviation between theory and experiment was previously observed in the determination of the dissociation energy for the $LiO^\bullet$ $^2\Pi$ radical. Specifically, Lee et al. computed a dissociation energy of 355.06 kJ mol^{-1} by means of an RCCSD(T) computation utilizing a quintuple-ζ quality basis set.[29] The experimental dissociation energy at 0 K was determined to be 336.8 ± 6.3 kJ mol^{-1} by Hildenbrand[97] from the ΔH^o_f for $LiO^\bullet$ (69.0 ± 6.3 kJ mol^{-1}).[93]

The difference between experiment and theory for the $LiO^\bullet$ radical was also previously highlighted by Langhoff et al.,[17] who noted that the experimentally derived separation between the $^2\Pi$ and $^2\Sigma^+$ states (30.68 kJ mol^{-1})[39,88] is similar to the difference between the theoretically and experimentally determined ΔH^o_f values for $LiO^\bullet$. Langhoff et al. suggested that the excited $A^2\Sigma^+$ state and not the ground $X^2\Pi$ state might have been prepared during the experiment that determined the ΔH^o_f for the $LiO^\bullet$ radical. Our results support this proposal. It seems reasonable to suggest that the experimental ΔH^o_f for the $X^2\Pi$ state of the $LiO^\bullet$ radical may need to be re-examined.

3.4. Predicted Ground States for MO^- and $MO^\bullet$. The information in Table 3 provides an ordering of the energies for the various states. For the radicals, the $^2\Pi$ state has been previously determined both theoretically[15,16,19,23,26−29,32] and experimentally[25,34,37−39] to be the ground state for $LiO^\bullet$ and $NaO^\bullet$. Our results agree with these previous studies, with the $^2\Pi$ state being 30.8 and 24.2 kJ mol^{-1} lower in energy than the $^2\Sigma^+$ state for $LiO^\bullet$ and $NaO^\bullet$, respectively. The situation for the $KO^\bullet$ ground state, however, is less clear, with the $^2\Sigma^+$ state lying only marginally lower than the $^2\Pi$ state, which is consistent with previous theoretical conclusions.[24,31]

To date, there has been less attention given to the ordering of states for MO^-.[24] For LiO^-, the ground state was previously determined to be $^3\Pi$.[24,33] Our calculations indicate that NaO^- also has a $^3\Pi$ ground state. However, the ground state of the anion changes for KO^-, with the $^1\Sigma^+$ state being the lowest in energy, as indicated by our multireference calculations. It should be noted that the single-reference W*n*C methods fail for the $^1\Sigma^+$ state due to the large multireference character of this state, with all of the W*n*C methods predicting a large negative enthalpy of formation. These results are in accord with the anionic ground states that were previously determined by Bauschlicher.[24] It is interesting to note that the four electronic states of KO^- lie within a range of just 5 kJ mol^{-1}.

3.5. State Separations. Separations between the low-lying states of the $MO^\bullet$ radicals and the MO^- anions, obtained at our three highest levels, are compared with available experimental data in Table 4.[98] For $LiO^\bullet$ and $NaO^\bullet$, all of the computed separations lie within 1−2 kJ mol^{-1} of the experimental values. For the $KO^\bullet$ radical, our general conclusion is that the $^2\Sigma^+$ and $^2\Pi$ states of $KO^\bullet$ lie very close in energy. The average of our W2C, W-ACPF, and W-AQCC results, determined using geometries optimized with CCSD(T)/AA′WCV5Z or MRCI+Q/AA′WCV5Z, indicates that the $^2\Sigma^+$ state lies lower in energy than the $^2\Pi$ state by 1.1 kJ mol^{-1}, and our best single-reference and multireference results all lie within 0.6 kJ mol^{-1} of this value. This state separation for $KO^\bullet$ is very slightly smaller than that reported in previous theoretical studies at the CCSD(T) level (e.g., 2.2 and 2.4 kJ mol^{-1}).[20,31]

All of the methods used to compute the $^3\Pi \rightarrow {}^3\Sigma^+$ state separation for LiO^-, NaO^-, and KO^- agree among themselves

TABLE 5: Electron Affinities (0 K, kJ mol^{-1}) for MO$^{\bullet}$

MO$^{\bullet}$	MO	W2C//CAA[a]	W-ACPF//MAA[b]	W-AQCC//MAA[c]	best estimate
LiO$^{\bullet}$ ($^2\Pi$)	$^3\Pi$	41.1	40.6	38.7	40.1
NaO$^{\bullet}$ ($^2\Pi$)	$^3\Pi$	53.6	52.9	50.8	52.4
KO$^{\bullet}$ ($^2\Pi$)	$^1\Sigma^+$	156.4	41.0	38.7	39.8
KO$^{\bullet}$ ($^2\Sigma^+$)	$^1\Sigma^+$	154.8	40.3	37.7	39.0

[a] W2C//CCSD(T)/AA′WCV5Z. [b] W2C-CAS-ACPF//MRCI+Q/AA′WCV5Z. [c] W2C-CAS-AQCC//MRCI+Q/AA′WCV5Z.

TABLE 6: Gas-Phase Acidities (0 K, kJ mol^{-1}) for MOH

MOH	MO$^-$	W2C//CAA[a]	W-ACPF//MAA[b]	W-AQCC//MAA[c]	best estimate
LiOH	$^3\Pi$	1778.0	1777.5	1779.3	1778.3
NaOH	$^3\Pi$	1751.5	1751.8	1754.2	1752.5
KOH	$^1\Sigma^+$	1654.7	1769.3	1771.5	1770.4

[a] W2C//CCSD(T)/AA′WCV5Z. [b] W2C-CAS-ACPF//MRCI+Q/AA′WCV5Z. [c] W2C-CAS-AQCC//MRCI+Q/AA′WCV5Z.

to within 1 kJ mol^{-1}. The $^1\Pi \rightarrow {}^1\Sigma^+$ separation, however, shows a much larger variation between the different methods, which may be attributed to the multireference character in the $^1\Sigma^+$ state that was noted earlier. For example, for LiO$^-$, this separation varies from 4.6 (W2C//CAA) to 15.1 (W-AQCC//MAA) kJ mol^{-1}, while for NaO$^-$, the corresponding separations are 3.5 (W2C//CAA) and 7.5 (W-AQCC//MAA) kJ mol^{-1}. For KO$^-$, W2C//CAA gives unmeaningful results because of the extreme problems in describing the $^1\Sigma^+$ state.

3.6. Electron Affinities. The calculated electron affinities (EA) of the metal monoxide radicals MO$^{\bullet}$, that is, the negative of the enthalpy change for the process MO$^{\bullet}$ + e $\rightarrow$ MO$^-$, are presented for our highest levels in Table 5.[98] As noted in section 3.4, the ground states of LiO$^{\bullet}$ and NaO$^{\bullet}$ have been theoretically and experimentally determined to be $^2\Pi$;[15,16,19,23,25−29,32,34,37−39] therefore, the EAs in Table 5 were calculated using the $^2\Pi$ state as the radical state in these cases. However, because there are two closely spaced low-lying states for the KO$^{\bullet}$ radical, Table 5 reports the EAs calculated for both the $^2\Pi$ and $^2\Sigma^+$ states of the radical.

The W2C//CAA, W-ACPF//MAA, and W-AQCC//MAA EAs for LiO$^{\bullet}$ and NaO$^{\bullet}$ lie within narrow ranges of 3 kJ mol^{-1}. However, because of problems with the $^1\Sigma^+$ state of KO$^-$, the W2C//CAA electron affinity is not meaningful.

Our best estimates for the EAs are 40.1, 52.4, and 39.0 kJ mol^{-1} for LiO$^{\bullet}$, NaO$^{\bullet}$, and KO$^{\bullet}$ ($^2\Sigma^+$), respectively. It is interesting that the EAs for LiO$^{\bullet}$ and KO$^{\bullet}$ lie within approximately 1 kJ mol^{-1} of one another while the EA for NaO$^{\bullet}$ is computed to be ~12 kJ mol^{-1} larger.

There have been few prior studies of the EAs for the alkali monoxide radicals with which to compare our results. Our best estimates of 40.1 kJ mol^{-1} for LiO$^{\bullet}$ and 52.4 kJ mol^{-1} for NaO$^{\bullet}$ compare well with previous high-level theoretical determinations.[22,24,33] Our calculated EA for LiO$^{\bullet}$ (40.1 kJ mol^{-1}) is consistent with the experimental observation[33] that LiO$^-$ transfers an electron to O_2 and therefore LiO$^{\bullet}$ must have an EA between 0 and 43.2 kJ mol^{-1} (the EA of O_2).

3.7. Gas-Phase Acidities. The calculated gas-phase acidities (ΔH_{acid}) of the alkali metal hydroxides, that is, the enthalpy changes for the reaction MOH $\rightarrow$ MO$^-$ + H$^+$, are shown for our highest levels in Table 6.[98] We note that a lower value for ΔH_{acid} corresponds to a more acidic MOH. For LiO$^-$ and NaO$^-$, the lowest electronic state is $^3\Pi$; therefore, the discussion of ΔH_{acid}(LiOH) and ΔH_{acid}(NaOH) will focus on lithium hydroxide and sodium hydroxide losing a proton to produce the $^3\Pi$ state of the MO$^-$ anion. For KO$^-$, the ground electronic state is the $^1\Sigma^+$ state, which possesses a large degree of multireference character. As a result, we have limited our discussion of ΔH_{acid}(KOH) to the results found by utilizing the multireference W-ACPF//MAA and W-AQCC//MAA methods. LiO$^-$ has recently been synthesized and found, on the basis of mass spectrometry experiments and high-level theoretical calculations, to be the strongest gas-phase base known.[33] Equivalently, LiOH is the weakest acid known.

Our best estimates for the ΔH_{acid} values for LiOH, NaOH, and KOH are 1778.3, 1752.5, and 1770.4 kJ mol^{-1}, respectively. These are in close agreement with previous high-level results for LiOH and NaOH.[33] Overall, the range of values obtained by the three (or two in the case of KOH) methods used to obtain these values spans less than 3.0 kJ mol^{-1}.

TABLE 7: Bond Dissociation Energies (0 K, kJ mol^{-1}) for MOH

MOH	MO$^{\bullet}$		W2C//CAA[a]	W-ACPF//MAA[b]	W-AQCC//MAA[c]	best estimate
LiOH	LiO$^{\bullet}$	$^2\Pi$	506.3	505.3	505.1	505.6
NaOH	NaO$^{\bullet}$	$^2\Pi$	492.3	492.0	492.1	492.1
KOH	KO$^{\bullet}$	$^2\Pi$	498.2	497.4	497.4	497.7
		$^2\Sigma^+$	496.6	496.7	496.5	496.6

[a] W2C//CCSD(T)/AA′WCV5Z. [b] W2C-CAS-ACPF//MRCI+Q/AA′WCV5Z. [c] W2C-CAS-AQCC//MRCI+Q/AA′WCV5Z.

3.8. Bond Dissociation Energies. The calculated bond dissociation energies (BDEs), that is, the enthalpy changes for the reaction MOH $\rightarrow$ MO$^{\bullet}$ + H$^{\bullet}$, are presented for our highest levels in Table 7.[98] We only consider dissociation to the ground $^2\Pi$ state for LiO$^{\bullet}$ and NaO$^{\bullet}$. For KO$^{\bullet}$, because the $^2\Sigma^+$ state is predicted to lie lower than the $^2\Pi$ state by only 1.1 kJ mol^{-1}, dissociations of KOH to both the $^2\Pi$ and $^2\Sigma^+$ electronic states of the radical are relevant.

Our best estimates of the BDEs for LiOH, NaOH, and KOH are 505.6, 492.1, and 497.7 ($^2\Pi$) and 496.6 ($^2\Sigma^+$) kJ mol^{-1}, respectively. In general, the three methods used to obtain these values give BDEs comparable to one another, with the largest variation being just 1.2 kJ mol^{-1}.

3.9. Comparison of the Alkali Metal Monoxide Anions, Monoxide Radicals, and Hydroxides. Selected structural and thermochemical properties of MO$^-$, MO$^{\bullet}$, and MOH are summarized in Table 8.

3.9.1. Molecular Orbital Description. A general molecular orbital scheme showing the result of the interaction of the orbitals of an alkali metal atom (M) with those of an oxygen atom to form an M−O bond is shown in Figure 1a. Interaction of the sp-type orbitals of the metal and the oxygen that point toward one another leads to the σ_1 bonding orbital, which is concentrated on O, and the σ_1* antibonding orbital, which is concentrated on M. The two sp-type orbitals that point away from one another are essentially nonbonding and give rise to the σ_2 orbital, which is slightly bonding and concentrated on O, and the σ_2* orbital, which is slightly antibonding and concentrated on M. The two p orbitals of the metal and oxygen interact to give the π bonding (concentrated on O) and the π* antibonding (concentrated on M) orbitals. Variable occupancy of the σ_2, π, and σ_2* orbitals gives rise to the various states of MO$^-$ and MO$^{\bullet}$.

3.9.2. Comparison of Bond Lengths. For all of the MO$^{\bullet}$ radicals, the $^2\Sigma^+$ state has a shorter M−O bond length than the $^2\Pi$ state. While the $^2\Pi$ state has an unpaired electron in the π orbital, the $^2\Sigma^+$ state has a partially occupied σ orbital (Figure 1b). Thus, it appears that full occupation of the π orbitals favors

TABLE 8: Summary of Best Calculated Thermochemical Predictions for MO^-, $MO^\bullet$, and MOH

molecule	M−O bond length ordering	state ordering	heat of formation[a] 298 K	heat of formation[a] 0 K	state separation ($\Pi \rightarrow \Sigma$)[b]	electron affinity[b]	acidity[b]	MO−H bond dissociation energy[b]
LiO^-	$^1\Sigma^+ < {}^3\Sigma^+ < {}^1\Pi \sim {}^3\Pi$	$^3\Pi < {}^1\Pi < {}^1\Sigma^+ < {}^3\Sigma^+$	8.5	8.5	13.1,[c] 33.1[d]			
$LiO^\bullet$	$^2\Sigma^+ < {}^2\Pi$	$^2\Pi < {}^2\Sigma^+$	48.5	48.6	30.8	40.1		
LiOH			−243.4	−241.0			1778.3	505.6
NaO^-	$^1\Sigma^+ < {}^3\Sigma^+ < {}^1\Pi \sim {}^3\Pi$	$^3\Pi < {}^1\Pi < {}^1\Sigma^+ < {}^3\Sigma^+$	34.2	35.4	7.4,[c] 22.1[d]			
$NaO^\bullet$	$^2\Sigma^+ < {}^2\Pi$	$^2\Pi < {}^2\Sigma^+$	86.4	87.9	24.2	52.4		
NaOH			−190.8	−188.2			1752.5	492.1
KO^-	$^1\Sigma^+ < {}^3\Sigma^+ < {}^1\Pi \sim {}^3\Pi$	$^1\Sigma^+ < {}^3\Pi < {}^1\Pi < {}^3\Sigma^+$	15.1	17.1	−3.3,[c] 1.92[d]			
$KO^\bullet$	$^2\Sigma^+ < {}^2\Pi$	$^2\Sigma^+ < {}^2\Pi$	55.9	57.9	−1.1	39.0		
KOH			−227.0	−222.7			1770.4	496.6

[a] Ground-state values. [b] 0 K. [c] Separation of singlet states. [d] Separation of triplet states.

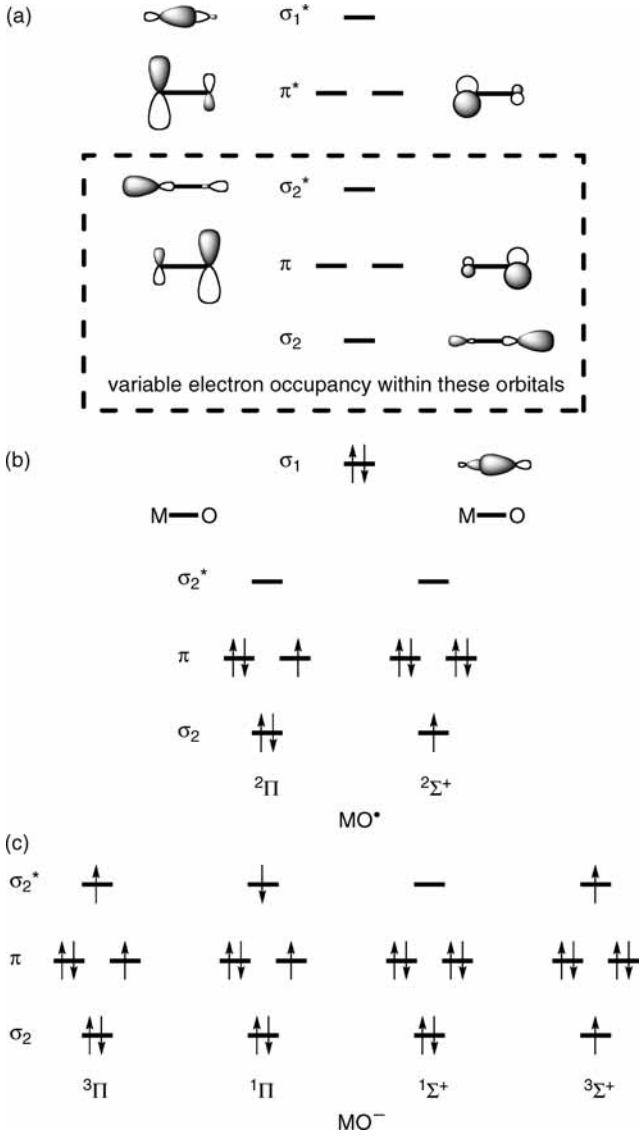

Figure 1. A qualitative representation of (a) the molecular orbitals derived from the interaction between the orbitals of an alkali metal atom (M) with those of an oxygen atom (O) and orbital occupancies for the various states of (b) $MO^\bullet$ and (c) MO^-.

a shorter M−O bond. For all of the MO^- anions, the M−O bond length increases in the order $^1\Sigma^+ < {}^3\Sigma^+ < {}^1\Pi \sim {}^3\Pi$. The fact that the Σ states have shorter bond lengths than the Π states is consistent with the Σ states having full occupation for the π bonding orbitals, whereas for the Π states, one of the π bonding orbitals is only singly occupied (Figure 1c). The M−O bond for the $^1\Sigma^+$ state is shorter than that for the $^3\Sigma^+$ state in all cases. This may be attributed to the slightly bonding σ_2 orbital being fully occupied in the $^1\Sigma^+$ state, while for the $^3\Sigma^+$ state, there is single occupancy of this orbital as well as the slightly antibonding σ_2* orbital.

3.9.3. Comparison of State Orderings. For the $MO^\bullet$ radicals, the $^2\Pi$ state lies lower in energy than the $^2\Sigma^+$ state for $LiO^\bullet$ and $NaO^\bullet$, whereas for $KO^\bullet$, as noted in section 3.4, the two states lie very close in energy, with the $^2\Sigma^+$ state being slightly lower. Similarly, for the LiO^- and NaO^- anions, the energy of the states increases in the order $^3\Pi < {}^1\Pi < {}^1\Sigma^+ < {}^3\Sigma^+$, while for KO^-, the $^1\Sigma^+$ state becomes the lowest in energy. The separation between the Π and the Σ states becomes less positive or more negative in the order Li > Na > K for both $MO^\bullet$ as well as for MO^-, that is, there is a relative favoring of the Σ states in going from Li to K.

Allison et al. provided a qualitative explanation for the observed change in the ground state of the $MO^\bullet$ radical as the size of the alkali metal increases[16] based on a balance between the Pauli repulsive forces and the quadrupole interactions. They noted that the Pauli repulsive term is smaller for the $^2\Sigma^+$ state than that for the $^2\Pi$ state and is proportional to $1/R_e$ (where R_e is the M−O bond length). On the other hand, the quadrupole term is repulsive for the $^2\Sigma^+$ state but decreases rapidly with increasing metal size because the interactions are proportional to $1/R_e^3$. Thus, when the metal is small and R_e is small, the $^2\Pi$ state lies lower in energy due to a dominant repulsive quadrupole term for the $^2\Sigma^+$ state. However, as the metal increases in size (leading to a larger R_e), the quadrupole interaction term becomes negligible, and the Pauli term, which favors the $^2\Sigma^+$ state, dominates.

The ordering of the states for both $MO^\bullet$ and MO^- can also be rationalized in terms of the nature of the M−O molecular orbitals shown in Figure 1. For $LiO^\bullet$ and $NaO^\bullet$, full occupation of the lower-energy σ_2 orbital leads to a $^2\Pi$ ground state. As the size of the metal increases and the metal becomes more electropositive, covalent interaction diminishes. As a result, occupation of the σ_2 orbital becomes relatively less favorable. This leads to a $^2\Sigma^+$ ground state.

Note that in all cases, that is, M = Li, Na, and K, the $MO^\bullet$ radical formally corresponds to $M^+O^{\bullet -}$. For MO^-, the $^1\Sigma^+$ state corresponds to M^+O^{2-}, whereas the $^3\Sigma^+$ and the Π states are formally $M^\bullet O^{\bullet -}$. As the alkali metal becomes larger and more electropositive, the $^1\Sigma^+$ state (M^+O^{2-}) can be expected to become increasingly favorable. This would account for the $^1\Sigma^+$ ground state for KO^- compared with the $^3\Pi$ ground states for LiO^- and NaO^-.

3.9.4. Comparison of Electron Affinities, Acidities and Bond Dissociation Energies. The electron affinities (EA) of $MO^\bullet$, the gas-phase acidities (ΔH_{acid}) of MOH, and the bond dissociation energies (BDEs) of the MO−H bond are associated with the heats of formation of $MO^\bullet$, MO^-, and MOH

$$\mathrm{EA(MO^{\bullet})} = \Delta H^{\circ}_{\mathrm{f}}(\mathrm{MO^{\bullet}}) - H^{\circ}_{\mathrm{f}}(\mathrm{MO^{-}})$$

$$\Delta H_{\mathrm{acid}}(\mathrm{MOH}) = \Delta H^{\circ}_{\mathrm{f}}(\mathrm{MO^{-}}) + \Delta H^{\circ}_{\mathrm{f}}(\mathrm{H^{+}}) - \Delta H^{\circ}_{\mathrm{f}}(\mathrm{MOH})$$

$$\mathrm{BDE(MO{-}H)} = \Delta H^{\circ}_{\mathrm{f}}(\mathrm{MO^{\bullet}}) + \Delta H^{\circ}_{\mathrm{f}}(\mathrm{H^{\bullet}}) - \Delta H^{\circ}_{\mathrm{f}}(\mathrm{MOH})$$

Thus, an understanding of the trends in the heats of formation of the constituent species assists in the understanding of the variations in the EA, ΔH_{acid}, and BDE values.

If we regard the heats of formation of a series of similar compounds as providing a measure of their relative stability, then $\mathrm{MO^{\bullet}}$, $\mathrm{MO^{-}}$, and MOH all become more stable in the order of Na < K < Li, as indicated by their heats of formation becoming less positive (for $\mathrm{MO^{\bullet}}$ and $\mathrm{MO^{-}}$) or more negative (for MOH) in this order. The nonmonotonic behavior in the sequence Li, Na, K indicates that two (or more) opposing effects are influencing the stabilities.

The M−O bond in $\mathrm{MO^{\bullet}}$ radicals can be represented by two major resonance structures representing the covalent and ionic contributions

$$\mathrm{M{-}O^{\bullet}} \leftrightarrow \mathrm{M^{+}\quad O^{\bullet -}}$$

As the size of the metal increases, the ionic contribution increases, contributing to a stronger bond. However, this occurs at the expense of decreasing overlap between M and O. These two opposing effects lead to the observed nonmonotonic trend in the stabilities (and hence the heats of formation) for $\mathrm{MO^{\bullet}}$ ($\mathrm{NaO^{\bullet}} < \mathrm{KO^{\bullet}} < \mathrm{LiO^{\bullet}}$). Such opposing effects for the M−O bond can also be employed to explain the similar trends in the heats of formation for $\mathrm{MO^{-}}$ and MOH.

The EAs of $\mathrm{MO^{\bullet}}$ lie within a relatively narrow range of 13.4 kJ $\mathrm{mol^{-1}}$ as the trends and degree of variations for $\Delta H^{\circ}_{\mathrm{f}}(\mathrm{MO^{\bullet}})$ and $\Delta H^{\circ}_{\mathrm{f}}(\mathrm{MO^{-}})$ are similar, with ranges of 37.9 and 25.7 kJ $\mathrm{mol^{-1}}$ for $\Delta H^{\circ}_{\mathrm{f}}(\mathrm{MO^{\bullet}})$ and $\Delta H^{\circ}_{\mathrm{f}}(\mathrm{MO^{-}})$, respectively. In a similar manner, there is a relatively small variation in the MO−H BDEs (a range of 13.5 kJ $\mathrm{mol^{-1}}$) owing to the similar degree of variations of 37.9 and 52.6 kJ $\mathrm{mol^{-1}}$, respectively, for $\Delta H^{\circ}_{\mathrm{f}}(\mathrm{MO^{\bullet}})$ and $\Delta H^{\circ}_{\mathrm{f}}(\mathrm{MOH})$. The ΔH_{acid} values of MOH span a wider range of 25.8 kJ $\mathrm{mol^{-1}}$. Intriguingly, the variation in $\Delta H_{\mathrm{acid}}(\mathrm{MOH})$ arises more because of the variation in $\Delta H^{\circ}_{\mathrm{f}}$ values for MOH (52.6 kJ $\mathrm{mol^{-1}}$) than because of the variation for $\mathrm{MO^{-}}$ (25.7 kJ $\mathrm{mol^{-1}}$).

4. Conclusions

The structures, enthalpies of formation ($\Delta H^{\circ}_{\mathrm{f}}$), state separations, electron affinities (EA), gas-phase acidities (ΔH_{acid}), and bond dissociation energies (BDE) associated with the alkali metal monoxide anions ($\mathrm{MO^{-}}$), monoxide radicals ($\mathrm{MO^{\bullet}}$), and hydroxides (MOH) (M = Li, Na, and K) have been examined using single- and multireference variants of the W*n*C methods based on geometries optimized with the A′WCV5Z and/or AA′WCV5Z basis sets. We find that these methods generally provide good agreement with available experimental data, though there are deviations of 20−30 kJ $\mathrm{mol^{-1}}$ between the W*n*C and experimental $\Delta H^{\circ}_{\mathrm{f}}$ values for the $\mathrm{LiO^{\bullet}}$ radical. We believe that re-examination of the experimental value for this species would be desirable.

In the case of the $^1\Sigma^+$ state of the $\mathrm{MO^{-}}$ anions, care needs to be taken because of possible significant multireference character, as indicated by the $\mathcal{T}_1$ diagnostic and the SCF contribution to the total atomization energy. The multireference character for this state for $\mathrm{KO^{-}}$ is reflected in the large deviations between results obtained using the single-reference W*n*C and multireference W2C-CAS methods for the enthalpy of formation.

The use of geometries optimized with augmented basis sets for the metal atom is found to have a significant effect in several cases, most noticeably for $\mathrm{KO^{-}}$. For example, the bond lengths in the various electronic states for $\mathrm{KO^{-}}$ are ∼0.02−0.04 Å shorter when the diffuse functions are included for the metal, with the most pronounced difference being 0.038 Å for the $^1\Sigma^+$ state. This leads to differences of 4−5 kJ $\mathrm{mol^{-1}}$ in estimates of the $\Delta H^{\circ}_{\mathrm{f}}$ values for $\mathrm{KO^{-}}$, obtained with A′WCV5Z and AA′WCV5Z geometries.

We find that for both $\mathrm{MO^{-}}$ and $\mathrm{MO^{\bullet}}$, the Σ states generally have shorter M−O distances than those for the Π states. For $\mathrm{LiO^{-}}$ and $\mathrm{NaO^{-}}$, the ground electronic state is determined to be $^3\Pi$, while the calculated ground state for $\mathrm{KO^{-}}$ is $^1\Sigma$. Similarly, we find that the $^2\Pi$ state is the ground state for $\mathrm{LiO^{\bullet}}$ and $\mathrm{NaO^{\bullet}}$, but for $\mathrm{KO^{\bullet}}$, the $^2\Sigma^+$ and $^2\Pi$ states lie very close in energy. Our best estimate is an energy difference of 1.1 kJ $\mathrm{mol^{-1}}$ in favor of the $^2\Sigma^+$ state. For both $\mathrm{MO^{-}}$ and $\mathrm{MO^{\bullet}}$, the separation of the states ($\Pi \rightarrow \Sigma$) becomes less positive or more negative as the size of the alkali metal increases, which manifests itself as a gradual change in the ground state from a Π state to a Σ state. The EAs for $\mathrm{MO^{\bullet}}$ and the BDEs for MO−H are found to vary in a narrow range of ∼13 kJ $\mathrm{mol^{-1}}$, while the magnitudes of $\Delta H_{\mathrm{acid}}(\mathrm{MOH})$ show a larger variation and follow the ordering of NaOH < KOH < LiOH, that is, LiOH is the weakest acid in the sequence. These observations can be rationalized through simple valence-bond considerations for the component $\mathrm{MO^{\bullet}}$, $\mathrm{MO^{-}}$, and MOH species.

Acknowledgment. A.K.W. gratefully acknowledges support from a National Science Foundation CAREER Award (CHE-0239555). Additional support was provided by the University of North Texas Academic Computing Services for the use of the UNT Research Cluster. Computational resources were also provided via a CRIF grant from the National Science Foundation (CHE-0342824) and by the National Computational Science Alliance under #CHE010021 and utilized the NCSA IBM p690. CASCaM is supported by a grant from the United States Department of Education. L.R. thanks Professor Jan Martin for the Dunham analysis program and gratefully acknowledges the award of an Australian Research Council Discovery Grant, funding from the ARC Centre of Excellence for Free Radical Chemistry and Biotechnology, and generous allocations of computing time from the National Computational Infrastructure (NCI) National Facility and the Australian Centre for Advanced Computing and Communications (AC3).

Supporting Information Available: Thermal corrections for enthalpies and calculated total energies for all species at the W1C, W2C, W-ACPF, and W-AQCC levels of theory (Table S1). $\mathcal{T}_1$ diagnostics and percent SCF contributions to the total atomization energies (Table S2). Full results for the separations of electronic states, electron affinities, gas-phase acidities, and bond dissociation energies (Tables S3−S6). This material is available free of charge via the Internet at http://pubs.acs.org.

References and Notes

(1) Kolb, C. E.; Elgin, J. B. *Nature* **1976**, *263*, 488.
(2) Ferguson, E. E. *Geophys. Res. Lett.* **1978**, *5*, 1035.
(3) Liu, S. C.; Reid, G. C. *Geophys. Res. Lett.* **1979**, *6*, 283.

(4) Murad, E.; Swider, W. *Geophys. Res. Lett.* **1979**, *6*, 929.
(5) Rowland, F. S.; Makide, Y. *Geophys. Res. Lett.* **1982**, *9*, 473.
(6) Scandrett, L. A.; Clift, R. *J. Inst. Energy* **1984**, *57*, 391.
(7) Osborn, G. A. *Fuel* **1992**, *71*, 131.
(8) Joo, S.; Worsnop, D. R.; Kolb, C. E.; Kim, S. K.; Herschbach, D. R. *J. Phys. Chem. A* **1999**, *103*, 3193.
(9) Konings, R. J. M.; Cordfunke, E. H. P. *J. Nucl. Mater.* **1989**, *167*, 251.
(10) Lin, W.; Krusholm, G.; Dam-Johansen, K.; Musahl, E.; Bank, L. *Proc. Int. Conf. Fluid Bed Combust.* **1997**, *14th*, 831.
(11) Oehman, M.; Nordin, A.; Skrifvars, B.-J.; Backman, R.; Hupa, M. *Energy Fuels* **2000**, *14*, 169.
(12) Chase Jr., M. W. *NIST-JANAF Themochemical Tables*, 4th ed.; American Institute of Physics: Melville, NY, 1998.
(13) O'Hare, P. A. G.; Wahl, A. C. *J. Chem. Phys.* **1972**, *56*, 4516.
(14) Yoshimine, M. *J. Chem. Phys.* **1972**, *57*, 1108.
(15) So, S. P.; Richards, W. G. *Chem. Phys. Lett.* **1975**, *32*, 227.
(16) Allison, J. N.; Cave, R. J.; Goddard, W. A., III. *J. Phys. Chem.* **1984**, *88*, 1262.
(17) Langhoff, S. R.; Bauschlicher, C. W., Jr.; Partridge, H. *J. Chem. Phys.* **1986**, *84*, 4474.
(18) Langhoff, S. R.; Partridge, H.; Bauschlicher, C. W., Jr. *Chem. Phys.* **1991**, *153*, 1.
(19) Lee, E. P. F.; Wright, T. G.; Dyke, J. M. *Mol. Phys.* **1992**, *77*, 501.
(20) Bauschlicher, C. W., Jr.; Partridge, H.; Dyall, K. G. *Chem. Phys. Lett.* **1992**, *199*, 225.
(21) Serrano-Andres, L.; Sanchez de Meras, A.; Pou-Amerigo, R.; Nebot-Gil, I. *THEOCHEM* **1992**, *86*, 229.
(22) Serrano-Andres, L.; Sanchez de Meras, A.; Pou-Amerigo, R.; Nebot-Gil, I. *Chem. Phys.* **1992**, *162*, 321.
(23) Boldyrev, A. I.; Simons, J.; Schleyer, P. v. R. *J. Chem. Phys.* **1993**, *99*, 8793.
(24) Bauschlicher, C. W., Jr.; Partridge, H.; Pettersson, L. G. M. *J. Chem. Phys.* **1993**, *99*, 3654.
(25) Pugh, J. V.; Shen, K. K.; Winstead, C. B.; Gole, J. L. *Chem. Phys.* **1996**, *202*, 129.
(26) Soldan, P.; Lee, E. P. F.; Wright, T. G. *J. Phys. Chem. A* **1998**, *102*, 9040.
(27) Lee, E. P. F.; Soldan, P.; Wright, T. G. *Chem. Phys. Lett.* **1998**, *295*, 354.
(28) Soldan, P.; Lee, E. P. F.; Gamblin, S. D.; Wright, T. G. *Phys. Chem. Chem. Phys.* **1999**, *1*, 4947.
(29) Lee, E. P. F.; Soldan, P.; Wright, T. G. *Chem. Phys. Lett.* **2001**, *347*, 481.
(30) Burk, P.; Sillar, K.; Koppel, I. A. *THEOCHEM* **2001**, *543*, 223.
(31) Lee, E. P. F.; Soldan, P.; Wright, T. G. *J. Chem. Phys.* **2002**, *117*, 8241.
(32) Lee, E. P. F.; Wright, T. G. *J. Phys. Chem. A* **2002**, *106*, 8903.
(33) Tian, Z.; Chan, B.; Sullivan, M. B.; Radom, L.; Kass, S. R. *Proc. Natl. Acad. Sci. U.S.A.* **2008**, *105*, 7647.
(34) Herm, R. R.; Herschbach, D. R. *J. Chem. Phys.* **1970**, *52*, 5783.
(35) Spiker, R. C., Jr.; Andrews, L. *J. Chem. Phys.* **1973**, *58*, 713.
(36) Lindsay, D. M.; Herschbach, D. R.; Kwiram, A. L. *J. Chem. Phys.* **1974**, *60*, 315.
(37) Pfeifer, J.; Gole, J. L. *J. Chem. Phys.* **1984**, *80*, 565.
(38) Woodward, J. R.; Hayden, J. S.; Gole, J. L. *Chem. Phys.* **1989**, *134*, 395.
(39) Yamada, C.; Fujitake, M.; Hirota, E. *J. Chem. Phys.* **1989**, *90*, 3033.
(40) Yamada, C.; Hirota, E. *J. Chem. Phys.* **1999**, *110*, 2853.
(41) Hirota, E. *Bull. Chem. Soc. Jpn.* **1995**, *68*, 1.
(42) Davidson, E. R.; Silver, D. W. *Chem. Phys. Lett.* **1977**, *52*, 403.
(43) Pople, J. A.; Head-Gordon, M.; Fox, D. J.; Raghavachari, K.; Curtiss, L. A. *J. Chem. Phys.* **1989**, *90*, 5622.
(44) Curtiss, L. A.; Jones, C.; Trucks, G. W.; Raghavachari, K.; Pople, J. A. *J. Chem. Phys.* **1990**, *93*, 2537.
(45) Curtiss, L. A.; Raghavachari, K.; Trucks, G. W.; Pople, J. A. *J. Chem. Phys.* **1991**, *94*, 7221.
(46) Curtiss, L. A.; Raghavachari, K.; Redfern, P. C.; Rassolov, V.; Pople, J. A. *J. Chem. Phys.* **1998**, *109*, 7764.
(47) Curtiss, L. A.; Redfern, P. C.; Raghavachari, K. *J. Chem. Phys.* **2005**, *123*, 124107/1.
(48) Curtiss, L. A.; Redfern, P. C.; Raghavachari, K. *J. Chem. Phys.* **2007**, *126*, 084108/1.
(49) Montgomery, J. A., Jr. ; Frisch, M. J.; Ochterski, J. W.; Petersson, G. A. *J. Chem. Phys.* **1999**, *110*, 2822.
(50) Montgomery, J. A., Jr.; Frisch, M. J.; Ochterski, J. W.; Petersson, G. A. *J. Chem. Phys.* **2000**, *112*, 6532.
(51) Wood, G. P. F.; Radom, L.; Petersson, G. A.; Barnes, E. C.; Frisch, M. J.; Montgomery, J. A., Jr. *J. Chem. Phys.* **2006**, *125*, 094106/1.
(52) Martin, J. M. L.; de Oliveira, G. *J. Chem. Phys.* **1999**, *111*, 1843.
(53) Parthiban, S.; Martin, J. M. L. *J. Chem. Phys.* **2001**, *114*, 6014.
(54) Boese, A. D.; Oren, M.; Atasoylu, O.; Martin, J. M. L.; Kallay, M.; Gauss, J. *J. Chem. Phys.* **2004**, *120*, 4129.
(55) Karton, A.; Rabinovich, E.; Martin, J. M. L.; Ruscic, B. *J. Chem. Phys.* **2006**, *125*, 144108/1.
(56) Tajti, A.; Szalay, P. G.; Csaszar, A. G.; Kallay, M.; Gauss, J.; Valeev, E. F.; Flowers, B. A.; Vazquez, J.; Stanton, J. F. *J. Chem. Phys.* **2004**, *121*, 11599.
(57) Szalay, P. G.; Tajti, A.; Stanton, J. F. *Mol. Phys.* **2005**, *103*, 2159.
(58) DeYonker, N. J.; Cundari, T. R.; Wilson, A. K. *J. Chem. Phys.* **2006**, *124*, 114104/1.
(59) DeYonker, N. J.; Cundari, T. R.; Wilson, A. K.; Sood, C. A.; Magers, D. H. *THEOCHEM* **2006**, *775*, 77.
(60) DeYonker, N. J.; Grimes, T.; Yockel, S.; Dinescu, A.; Mintz, B.; Cundari, T. R.; Wilson, A. K. *J. Chem. Phys.* **2006**, *125*, 104111/1.
(61) DeYonker, N. J.; Ho, D. S.; Wilson, A. K.; Cundari, T. R. *J. Phys. Chem. A* **2007**, *111*, 10776.
(62) DeYonker, N. J.; Peterson, K. A.; Steyl, G.; Wilson, A. K.; Cundari, T. R. *J. Phys. Chem. A* **2007**, *111*, 11269.
(63) Martin, J. M. L. *Chem. Phys. Lett.* **1999**, *303*, 399.
(64) Martin, J. M. L.; Parthiban, S. In *Quantum-Mechanical Prediction of Thermochemical Data*; Cioslowski, J., Ed.; Kluwer Academic: Dordrecht, The Netherlands, 2001.
(65) Martin, J. M. L. *Spectrochim. Acta, Part A* **2001**, *57A*, 875.
(66) Schulz, A.; Smith, B. J.; Radom, L. *J. Phys. Chem. A* **1999**, *103*, 7522.
(67) Sullivan, M. B.; Iron, M. A.; Redfern, P. C.; Martin, J. M. L.; Curtiss, L. A.; Radom, L. *J. Phys. Chem. A* **2003**, *107*, 5617.
(68) Dunning, T. H., Jr. *J. Chem. Phys.* **1989**, *90*, 1007.
(69) Wilson, A. K.; Woon, D. E.; Peterson, K. A.; Dunning, T. H., Jr. *Book of Abstracts*; 213th ACS National Meeting, San Francisco, April 13−17 1997; PHYS 060.
(70) Wilson, A. K.; Woon, D. E.; Peterson, K. A.; Dunning, T. H., Jr. *J. Chem. Phys.* **1999**, *110*, 7667.
(71) Dunning, T. H., Jr.; Peterson, K. A.; Wilson, A. K. *J. Chem. Phys.* **2001**, *114*, 9244.
(72) Woon, D. E.; Dunning, T. H., Jr. *J. Chem. Phys.* **1994**, *100*, 2975.
(73) Woon, D. E.; Dunning, T. H., Jr. *J. Chem. Phys.* **1995**, *103*, 4572.
(74) Peterson, K. A.; Dunning, T. H., Jr. *J. Chem. Phys.* **2002**, *117*, 10548.
(75) Iron, M. A.; Oren, M.; Martin, J. M. L. *Mol. Phys.* **2003**, *101*, 1345.
(76) Frisch, M. J.; Trucks, G. W.; Schlegel, H. B.; Scuseria, G. E.; Robb, M. A.; Cheeseman, J. R.; Montgomery, J. A., Jr.; Vreven, T.; Kudin, K. N.; Burant, J. C.; Millam, J. M.; Iyengar, S. S.; Tomasi, J.; Barone, V.; Mennucci, B.; Cossi, M.; Scalmani, G.; Rega, N.; Petersson, G. A.; Nakatsuji, H.; Hada, M.; Ehara, M.; Toyota, K.; Fukuda, R.; Hasegawa, J.; Ishida, M.; Nakajima, T.; Honda, Y.; Kitao, O.; Nakai, H.; Klene, M.; Li, X.; Knox, J. E.; Hratchian, H. P.; Cross, J. B.; Bakken, V.; Adamo, C.; Jaramillo, J.; Gomperts, R.; Stratmann, R. E.; Yazyev, O.; Austin, A. J.; Cammi, R.; Pomelli, C.; Ochterski, J. W.; Ayala, P. Y.; Morokuma, K.; Voth, G. A.; Salvador, P.; Dannenberg, J. J.; Zakrzewski, V. G.; Dapprich, S.; Daniels, A. D.; Strain, M. C.; Farkas, O.; Malick, D. K.; Rabuck, A. D.; Raghavachari, K.; Foresman, J. B.; Ortiz, J. V.; Cui, Q.; Baboul, A. G.; Clifford, S.; Cioslowski, J.; Stefanov, B. B.; Liu, G.; Liashenko, A.; Piskorz, P.; Komaromi, I.; Martin, R. L.; Fox, D. J.; Keith, T.; Al-Laham, M. A.; Peng, C. Y.; Nanayakkara, A.; Challacombe, M.; Gill, P. M. W.; Johnson, B.; Chen, W.; Wong, M. W.; Gonzalez, C.; Pople, J. A. *Gaussian 03*, revision C.02; Gaussian, Inc.: Wallingford, CT, 2004.
(77) Werner, H.-J.; Knowles, P. J.; Lindh, R.; Manby, F. R.; Schütz, M.; Celani, P.; Korona, T.; Mitrushenkov, A.; Rauhut, G.; Adler, T. B.; Amos, R. D.; Bernhardsson, A.; Berning, A.; Cooper, D. L.; Deegan, M. J. O.; Dobbyn, A. J.; Eckert, F.; Goll, E.; Hampel, C.; Hetzer, G.; Hrenar, T.; Knizia, G.; Köppl, C.; Liu, Y.; Lloyd, A. W.; Mata, R. A.; May, A. J.; McNicholas, S. J.; Meyer, W.; Mura, M. E.; Nicklaβ, A.; Palmieri, P.; Pflüger, K.; Pitzer, R.; Reiher, M.; Schumann, U.; Stoll, H.; Stone, A. J.; Tarroni, R.; Thorsteinsson, T.; Wang, M.; Wolf, A. MOLPRO 2002.6; University of Birmingham: Birmingham, U.K., 2002.
(78) Nicolaides, A.; Rauk, A.; Glukhovtsev, M. N.; Radom, L. *J. Phys. Chem.* **1996**, *100*, 17460.
(79) Dunham, J. L. *Phys. Rev.* **1932**, *41*, 713.
(80) Gdanitz, R. J.; Ahlrichs, R. *Chem. Phys. Lett.* **1988**, *143*, 413.
(81) Gdanitz, R. J. *Int. J. Quantum Chem.* **2001**, *85*, 281.
(82) Cowan, R. D.; Griffin, D. C. *J. Opt. Soc. Am.* **1976**, *66*, 1010.
(83) Martin, R. L. *J. Phys. Chem.* **1983**, *87*, 750.
(84) Lee, T. J.; Taylor, P. R. *Int. J. Quantum Chem., Quantum Chem. Symp.* **1989**, *23*, 199.
(85) Szalay, P. G.; Bartlett, R. J. *Chem. Phys. Lett.* **1993**, *214*, 481.
(86) Szalay, P. G.; Bartlett, R. J. *J. Chem. Phys.* **1995**, *103*, 3600.
(87) Fuesti-Molnar, L.; Szalay, P. G. *J. Phys. Chem.* **1996**, *100*, 6288.
(88) Yamada, C.; Fujitake, M.; Hirota, E. *J. Chem. Phys.* **1989**, *91*, 137.
(89) Kuchitsu, K., Ed. *Landolt-Bornstein: Group II: Molecules and Radicals; Volume 25/A: Structure Data of Free Polyatomic Molecules,*

Supplemented and Revised Edition, Inorganic Molecules; Springer: Berlin, Germany, 1998.

(90) Huber, K. P.; Herzberg, G. In *NIST Chemistry WebBook*, NIST Standard Reference Database Number 69; Linstrom, P. J., Mallard, W. G., Eds.; National Institute of Standards and Technology: Gaithersburg, MD, 2009.

(91) Ehlert, T. C. *High Temp. Sci.* **1977**, *9*, 237.

(92) Pedley, J. B.; Marshall, E. M. *J. Phys. Chem. Ref. Data* **1983**, *12*, 967.

(93) Lamoreaux, R. H.; Hildenbrand, D. L. *J. Phys. Chem. Ref. Data* **1984**, *13*, 151.

(94) Farber, M.; Srivastava, R. D. *High Temp. High Pressures* **1988**, *20*, 119.

(95) Steinberg, M.; Schofield, K. *J. Chem. Phys.* **1991**, *94*, 3901.

(96) Gurvich, L. V.; Bergman, G. A.; Gorokhov, L. N.; Iorish, V. S.; Leonidov, V. Y.; Yungman, V. S. *J. Phys. Chem. Ref. Data* **1996**, *25*, 1211.

(97) Hildenbrand, D. L. *J. Chem. Phys.* **1972**, *57*, 4556.

(98) Results at all seven theoretical levels are included in Tables S3 (state separations), S4 (electron affinities), S5 (gas-phase acidities), and S6 (bond dissociation energies) of the Supporting Information.

JP9034826